Synthesis of Advanced Microwave Filters Without Diagonal Cross-Couplings

Richard J. Cameron, *Fellow, IEEE,* A. R. Harish, *Member, IEEE,* and Christopher J. Radcliffe, *Member, IEEE*

***Abstract*—Asymmetric filtering characteristics are frequently used for the design of microwave filters for the cellular telephony industry, particularly for the transmit/receive diplexers for base stations. Typically, such filters have to be manufactured in large quantities at the lowest possible cost. However, due to the asymmetric filtering characteristics, the designs often include diagonal cross-couplings between nonadjacent resonators in addition to the usual "straight" couplings. Diagonal couplings tend to be mechanically difficult to manufacture and assemble and can be electrically awkward to tune and be sensitive to temperature, vibration, etc., all of which drives up unit costs. This paper introduces the methods for the synthesis of two novel filter network configurations that do not require diagonal couplings, but nonetheless are able to realize asymmetric filtering functions.**

***Index Terms*—Asymmetric filtering functions, Chebyshev characteristics, circuit synthesis methods, coupling matrix, cross-couplings, microwave filters.**

I. Introduction

IN ORDER TO cope with the increasing demand for capacity in restricted spectral bandwidths, specifications for channelizing filter rejections have tended to become asymmetric. This is particularly true for the front-end transmit/receive diplexers in the base stations of mobile communications systems and requires the use of advanced filtering characteristics, optimally tailored to the rejection requirements, whilst at the same time, maintaining maximum in-band amplitude and group-delay linearity and lowest insertion loss.

In the course of synthesizing the networks for such characteristics and then reconfiguring the inter-resonator main line and cross-couplings to give a convenient realization, it is frequently found that diagonal couplings are required. Diagonal couplings are those that interconnect resonators arranged in a grid pattern at an angle relative to the grid lines, where "straight" couplings are parallel to the grid lines (e.g., Fig. 1).

In this paper, two novel synthesis methods are presented that allow the realization of symmetric or asymmetric filtering characteristics without the need for diagonal cross-couplings. The first is the "box" configuration and a derivation known as the "extended box" configuration, and the second is the "cul-de-sac" filter configuration.

Manuscript received April 1, 2002; revised August 19, 2002.

R. J. Cameron is with COM DEV International Ltd., Aylesbury HP22 5SX, U.K.

A. R. Harish is with the Indian Institute of Technology, Kanpur 208016, India.

C. J. Radcliffe is with Pentire Associates, Bedford MK45 4NR, U.K.

Digital Object Identifier 10.1109/TMTT.2002.805141

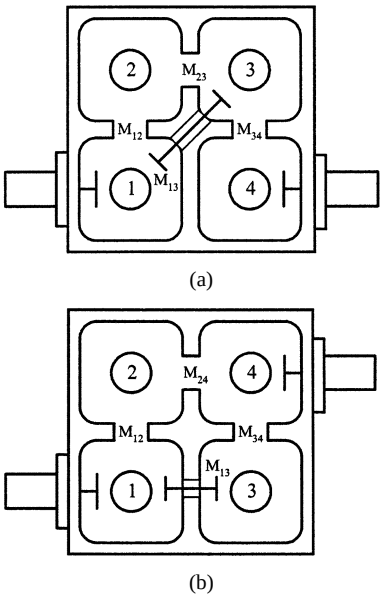

Fig. 1. 4–1 asymmetric filtering function. (a) Realized with conventional diagonal cross-coupling (M_{13}). (b) Realized with the box configuration.

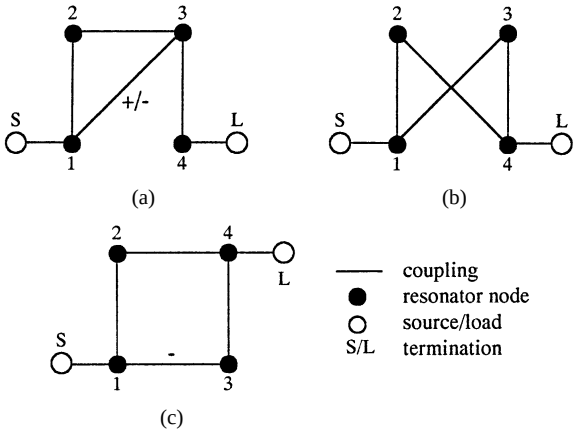

Fig. 2. 4–1 filter: formation of the box section. (a) Trisection. (b) Annihilation of M_{23} and creation of M_{24}. (c) "Untwisting" to obtain box section.

II. Box Sections

The box section is similar to the cascade quartet section [5], i.e., four resonator nodes arranged in a square formation, but with the input to and the output from the quartet from opposite corners of the square. Fig. 1(a) shows the conventional quartet arrangement for a fourth degree filtering characteristic with a single transmission zero (TZ), realized with the diagonal cross-coupling M_{13} (a "trisection," see [1]). Fig. 1(b) shows the equivalent box section realizing the same TZ, but without the

	S	1	2	3	4	L
S	0	1.1506	0	0	0	0
1	1.1506	0.0530	0.9777	0.3530	0	0
2	0	0.9777	–0.4198	0.7128	0	0
3	0	0.3530	0.7128	0.0949	1.0394	0
4	0	0	0	1.0394	0.0530	1.1506
L	0	0	0	0	1.1506	0

(a)

	S	1	2	3	4	L
S	0	1.1506	0	0	0	0
1	1.1506	0.0530	0.5973	–0.8507	0	0
2	0	0.5973	–0.9203	0	0.5973	0
3	0	–0.8507	0	0.5954	0.8507	0
4	0	0	0.5973	0.8507	0.0530	1.1506
L	0	0	0	0	1.1506	0

(b)

	S	1	2	3	4	L
S	0	1.1506	0	0	0	0
1	1.1506	–0.0530	0.5973	–0.8507	0	0
2	0	0.5973	0.9203	0	0.5973	0
3	0	–0.8507	0	–0.5954	0.8507	0
4	0	0	0.5973	0.8507	–0.0530	1.1506
L	0	0	0	0	1.1506	0

(c)

Fig. 3. 4–1 filter: coupling matrices. (a) Trisection. (b) After transformation to box section (TZ on upper side of passband). (c) TZ on lower side of passband.

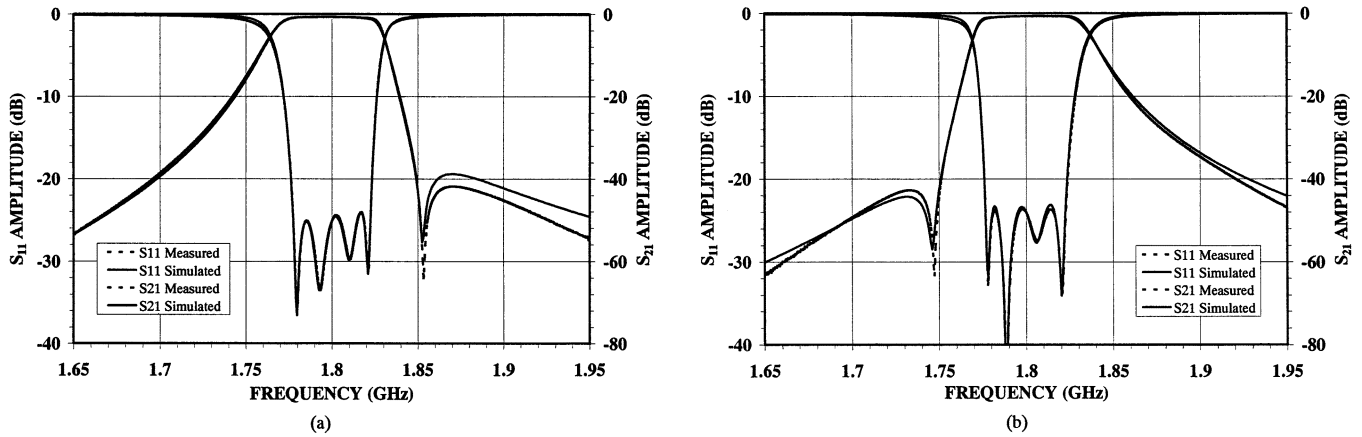

Fig. 4. 4–1 filter: measured results. (a) TZ on upper side. (b) TZ on lower side.

need for the diagonal coupling. Application of the "minimum path" rule indicates that the box section can realize only a single TZ.

The box section is created by the application of a "cross-pivot" similarity transform to a trisection [1] in the coupling matrix for the filter. A cross-pivot similarity transform is the case where the coordinates of the coupling matrix element to be annihilated are the same as the pivot of the transform itself, i.e., the element to be annihilated lies on the cross-points of the pivot. The angle of the similarity transform for the annihilation of an element M_{ij} at the pivot cross-point (i, j) is different to that of a regular annihilation [2] and is given by

$$\theta_r = \frac{1}{2}\tan^{-1}\left[\frac{2M_{ij}}{(M_{jj} - M_{ii})}\right] + \frac{k\pi}{2} \tag{1}$$

where i and j are the coordinates of the pivot and also of the element to be annihilated, θ_r is the angle of the similarity transform, and k is an arbitrary integer. For the box section, the pivot is set to annihilate the second main line coupling of the trisection in the coupling matrix, i.e., $i = 2$ and $j = 3$ in the fourth degree example of Fig. 1 and its equivalent coupling and routing schematic [see Fig. 2(a)]. In the process of annihilating the main line coupling M_{23}, the coupling M_{24} is created [see Fig. 2(b)] and then by "untwisting" this section, the box section is formed [see Fig. 2(c)]

In the resultant box section, one of the couplings will always be negative, irrespective of the sign of the cross-coupling (M_{13}) in the original trisection.

To illustrate the procedure, an example is taken of a fourth degree 25-dB return-loss Chebyshev filtering characteristic, with a single TZ at $s = +j2.3940$ to give a lobe level of 41 dB on the upper side of the passband.

Fig. 3(a) below gives the "$N+2$" coupling matrix for the 4–1 filter showing the M_{13} trisection cross-coupling, corresponding to the coupling diagram of Fig. 2(a). Fig. 3(b) shows the coupling matrix after transformation to the box configuration. Fig. 4 shows the measured results of a coaxial resonator realization of

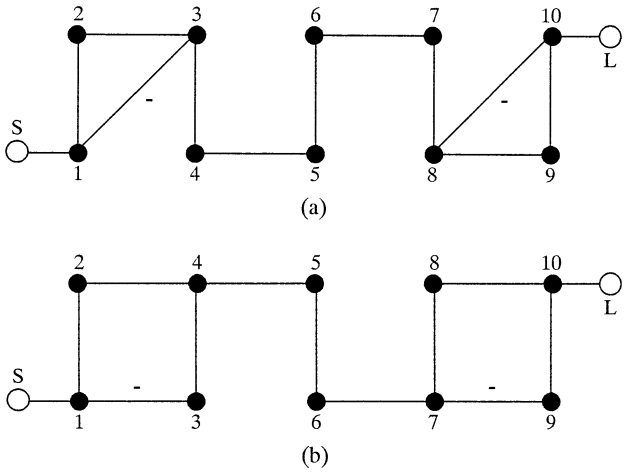

Fig. 5. 10–2 asymmetric filter: coupling and routing diagrams. (a) Synthesized with two trisections. (b) After transformation of trisections to two box sections by application of two cross-pivot rotations at pivots $[2, 3]$ and $[8, 9]$. This form is suitable for realization in dual-mode technology.

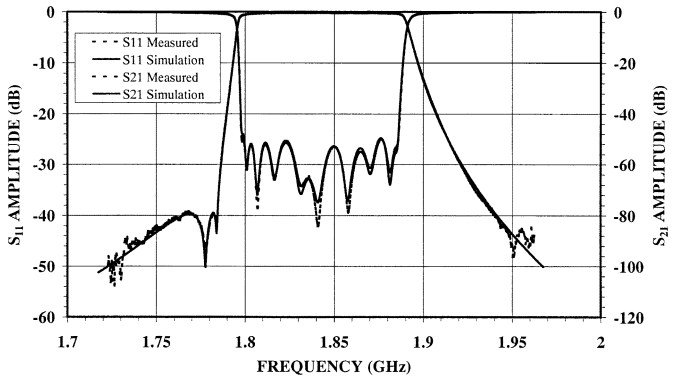

Fig. 6. 10–2 asymmetric filter: RF simulated and measured return loss and rejection.

the 4–1 filter configured as in Fig. 1(b). Good correlation is obtained between the measured and simulated results.

If the TZ is placed at $-j2.3940$ below the passband instead of above, then the transformation to the box section will result in the same values for the inter-resonator couplings, but complementary values for the self-couplings [$M_{11}, M_{22}, \ldots$, etc. along the principal diagonal of the coupling matrix, see Fig. 3(c)]. Since the self-couplings represent offsets from center frequency and are adjustable by tuning screws, it means that the same filter structure may be used, for example, for the complementary filters of a transmit (Tx)/receive (Rx) diplexer. Fig. 4(b) shows the measured results of the same structure that gave the single TZ on the upper side of the passband [see Fig. 4(a)], now retuned to place the TZ below the passband.

Box sections may also be cascaded within higher degree filters, indexing the coordinates of the pivots in (1) appropriately to correspond correctly with the position of each trisection. Fig. 5 gives the coupling and routing diagrams for a tenth degree example with two TZs on the lower side of the passband, while Fig. 6 shows the measured and simulated return loss and rejection characteristics of a test filter.

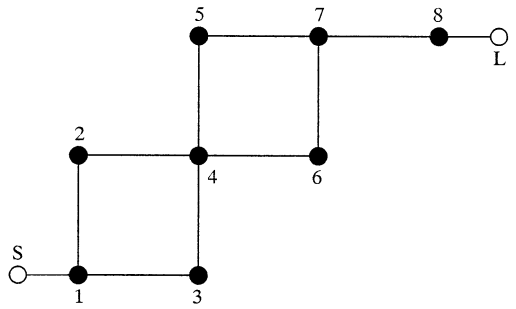

Fig. 7. Eighth degree network. Two box sections conjoined at one corner.

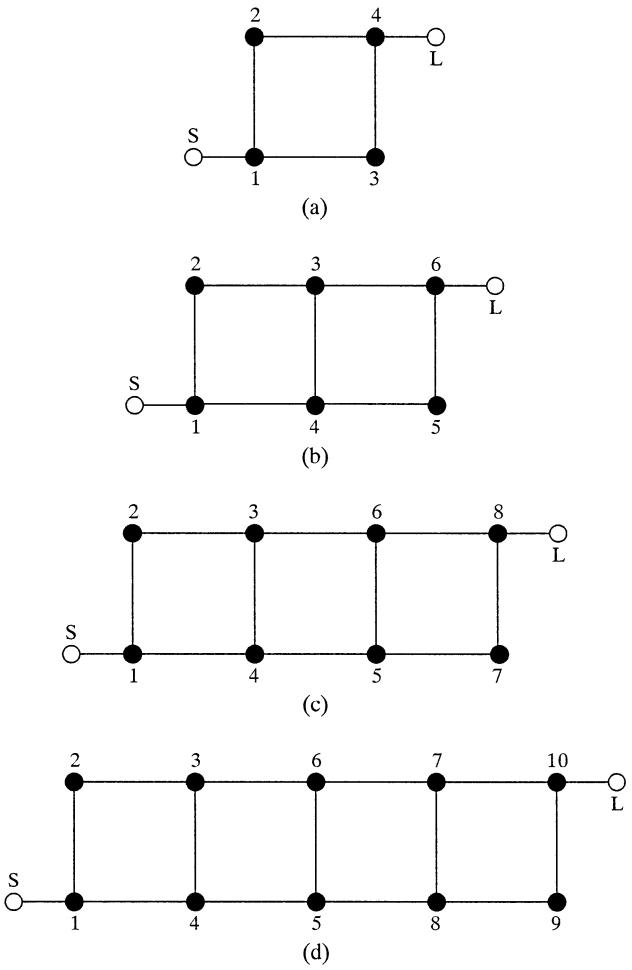

Fig. 8. Coupling and routing diagrams for extended box-section networks. (a) Fourth degree (basic box section). (b) Sixth degree. (c) Eighth degree. (d) Tenth degree.

It may be seen from Fig. 5(b) that because there are no diagonal cross-couplings, it would be possible to realize this asymmetric characteristic in dual-mode cavities

III. Extended Box Sections

A series of box sections may be formed in higher degree networks by cascading trisections and applying the single cross-pivot rotation to eliminate the main-line coupling within each one and then untwisting. However, the closest that box sections may be created by this method is where two sections share a common resonator, e.g., the eighth degree network of Fig. 7.

TABLE I
PIVOT COORDINATES FOR THE REDUCTION OF THE FOLDED MATRIX TO THE EXTENDED BOX-SECTION CONFIGURATION—SIXTH, EIGHTH, AND TENTH DEGREES

Degree N	Rotation No. r	Rotation Pivot $[i, j]$	Angle θ_r	Annihilating Element(s):
6	1	[3, 4]	θ_1	–
	2	[2, 4]		M_{24}
	3	[3, 5]		M_{25} and M_{35}
8	1	[4, 5]	θ_1	–
	2	[5, 6]	θ_2	–
	3	[3, 5]		M_{37}
	4	[3, 4]		M_{46}
	5	[3, 5]		M_{35}
	6	[2, 4]		M_{24} and M_{25}
	7	[6, 7]		M_{67} and M_{37}
10	1	[5, 6]	θ_1	–
	2	[5, 7]	θ_2	–
	3	[6, 7]	θ_3	–
	4	[4, 7]	θ_4	–
	5	[4, 6]	θ_5	–
	6	[4, 5]		M_{47}
	7	[6, 8]		M_{48}
	8	[3, 5]		M_{37} and M_{38}
	9	[7, 8]		M_{57} and M_{68}
	10	[3, 4]		M_{46} and M_{35}
	11	[7, 9]		M_{79} and M_{69}
	12	[2, 4]		M_{24} and M_{25}

This leads to a rather awkward and restricted layout and heavily loads the common resonator (resonator 4 of Fig. 7) with four couplings. Moreover, only two TZs may be realized by this network.

A rather more convenient arrangement both in physical layout and number of TZs that may be realized is shown in Fig. 8. Here, the basic fourth degree box section is shown and then the addition of pairs of resonators to form sixth, eighth, and tenth degree networks. Application of the minimum path rule indicates that a maximum of 1, 2, 3, or 4 TZs may be realized by the fourth, sixth, eighth, and tenth degree networks, respectively. The resonators are arranged in two parallel rows with half the total number of resonators in each row, input is at the corner at one end, and output from the diagonally opposite corner at the other end. Even though asymmetric characteristics may be prescribed, there are no diagonal cross-couplings.

There appears to be no regular pattern for determining the sequence of rotations to synthesize the coupling matrix for the extended box sections from the folded network or any other canonical network. The sequences that are shown in Table I were derived by first determining the sequence of rotations to reduce the extended box-section network to the corresponding folded network coupling matrix, for which a regular procedure exists [2]. This sequence of rotations is then reversed to transform the folded coupling matrix (which is readily derived from the S_{21} and S_{11} polynomials using the methods of [2] or [3] and [4]) back to the box-section matrix.

Reversing the sequence means that some of the rotation angles θ_r are unknown *a priori* and can only be determined by relating the coupling elements of the final matrix with those of the initial folded matrix and then solving to find the θ_r (similar to the procedure for synthesizing cascade quadruplets in an eighth degree network, see [5]). Deriving the equations to solve for θ_r analytically involves a formidable amount of algebra and the task becomes most easily performed by setting up a simple solver procedure.

The procedure starts by setting initial values for the unknown rotation angles (one for the sixth degree, two for the eighth degree, and five for the tenth degree) and then running through the sequence of rotations, as shown in Table I, to obtain the transformed coupling matrix. With these initial angles, some of the unwanted coupling matrix elements will have nonzero values and a cost function may be evaluated by forming, for example, the root–sum–square of the values of all the elements in the coupling matrix that should be zero. The initial angles may then be adjusted by the solver routine until the cost function is zero. By varying the value of the integer k in the cross-pivot angle formula (1), when it is used in the rotation sequences, several unique solutions may be found in most cases, allowing the choice of the coupling matrix that gives the most convenient coupling values for the technology to be used for the realization.

An example is taken of an eighth degree filtering characteristic with 23-dB return loss and three prescribed TZs at $s = -j1.3553$, $+j1.1093$, and $+j1.2180$, which produce one rejection lobe level of 40 dB on the lower side of the passband and two at 40 dB on the upper side. The folded "$N + 2$" coupling matrix is shown in Fig. 9(a), and having found the two unknown angles θ_1 and θ_2 of one of the possible solutions ($+63.881°$ and $+35.865°$, respectively) and applying the sequence of seven rotations (Table I), the coupling matrix for the extended box section is obtained [see Fig. 9(b)], which corresponds to the coupling and routing diagram of Fig. 8(c). The analyzed transfer and reflection characteristics for this coupling matrix are shown in Fig. 10, demonstrating that the performance has been preserved intact.

It may be seen from Fig. 8 that because they have no diagonal cross-couplings, extended box sections are also very suitable for realization with dual-mode resonator cavities. A practical ad-

	S	1	2	3	4	5	6	7	8	L
S	0	1.0428	0	0	0	0	0	0	0	0
1	1.0428	0.0107	0.8623	0	0	0	0	0	0	0
2	0	0.8623	0.0115	0.5994	0	0	0	0	0	0
3	0	0	0.5994	0.0133	0.5356	0	–0.0457	–0.1316	0	0
4	0	0	0	0.5356	0.0898	0.3361	0.5673	0	0	0
5	0	0	0	0	0.3361	–0.8513	0.3191	0	0	0
6	0	0	0	–0.0457	0.5673	0.3191	–0.0073	0.5848	0	0
7	0	0	0	–0.1316	0	0	0.5848	0.0115	0.8623	0
8	0	0	0	0	0	0	0	0.8623	0.0107	1.0428
L	0	0	0	0	0	0	0	0	1.0428	0

(a)

	S	1	2	3	4	5	6	7	8	L
S	0	1.0428	0	0	0	0	0	0	0	0
1	1.0428	0.0107	0.2187	0	–0.8341	0	0	0	0	0
2	0	0.2187	–1.0053	0.0428	0	0	0	0	0	0
3	0	0	0.0428	–0.7873	0.2541	0	–0.2686	0	0	0
4	0	–0.8341	0	0.2541	0.0814	0.4991	0	0	0	0
5	0	0	0	0	0.4991	0.2955	0.4162	0.1937	0	0
6	0	0	0	–0.2686	0	0.4162	–0.2360	0	–0.7644	0
7	0	0	0	0	0	0.1937	0	0.9192	0.3991	0
8	0	0	0	0	0	0	–0.7644	0.3991	0.0107	1.0428
L	0	0	0	0	0	0	0	0	1.0428	0

(b)

Fig. 9. Extended box-section configuration: eighth degree example. (a) Original folded coupling matrix. (b) After transformation to extended box-section configuration.

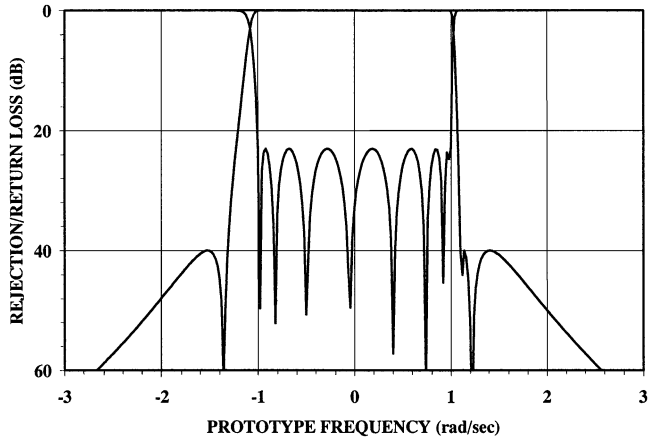

Fig. 10. 8–3 asymmetric filter in extended box-section configuration: simulated rejection and return-loss performance.

vantage arises from all the straight couplings being present, in that any spurious stray couplings become less significant. Seventh, ninth, and eleventh odd-degree filters may also be synthesized, using the rotation sequences for the sixth, eighth, and tenth degree filters, respectively.

By working on subsections of the main coupling matrix, hybrid forms may also be created. An example is given of an eleventh degree characteristic with three Tx zeros, which may be initially synthesized with three trisections [see Fig. 11(a)]. The first two trisections are then transformed into an asymmetric cascade quad section with two similarity transforms at pivots $[4, 5]$ and $[3, 4]$ to eliminate couplings M_{46} and M_{24}, respectively [2]. The iterative procedure described above for the sixth degree case may then be applied to the upper left 6×6 submatrix of the main matrix to form the extended box section at the left-hand side of the network [see Fig. 11(b)]. Finally, the basic box section at the right-hand side may be formed with a cross-pivot transform at pivot $[8, 9]$ to eliminate coupling M_{89}. Alternatively, applying the cross-pivot transform at pivot $[9, 10]$ would form the basic box section at the extreme right of the network.

IV. Cul-de-Sac Configuration

The cul-de-sac configuration is restricted to double-terminated networks and will realize a maximum of $N-3$ TZs. Otherwise it will accommodate any even- or odd-degree symmetric or asymmetric prototype. Moreover, its form lends itself to a certain amount of flexibility in the physical layout of its resonators [6].

A typical cul-de-sac configuration is shown in Fig. 12(a) for a tenth degree prototype with the maximum-allowable seven Tx zeros (in this case, three imaginary-axis and two complex pairs). There is a central "core" of a quartet of resonators in a square formation [1, 2, 9, and 10 in Fig. 12(a)], straight-coupled to each other (i.e., no diagonal cross-couplings). One of these couplings is always negative; the choice of which one is arbitrary. The entry to and exit from the core quartet are from opposite corners of the square [1 and 10, respectively, in Fig. 12(a)].

Some or all of the rest of the resonators are strung out in cascade from the other two corners of the core quartet in equal numbers (even-degree prototypes) or one more than the other (odd-degree prototypes). The last resonator in each of the two chains has no output coupling; hence, the nomenclature "cul-de-sac" for this configuration. Other possible configurations are shown in Fig. 12(b) (eighth degree) and Fig. 12(c) (seventh degree). If it is practical to include a diagonal cross-coupling between the input and output of the core quartet, an extra TZ may be realized. This coupling will have the same value as in the original folded coupling matrix.

The procedure for the synthesis of the cul-de-sac network takes advantage of the symmetry of the ladder lattice network

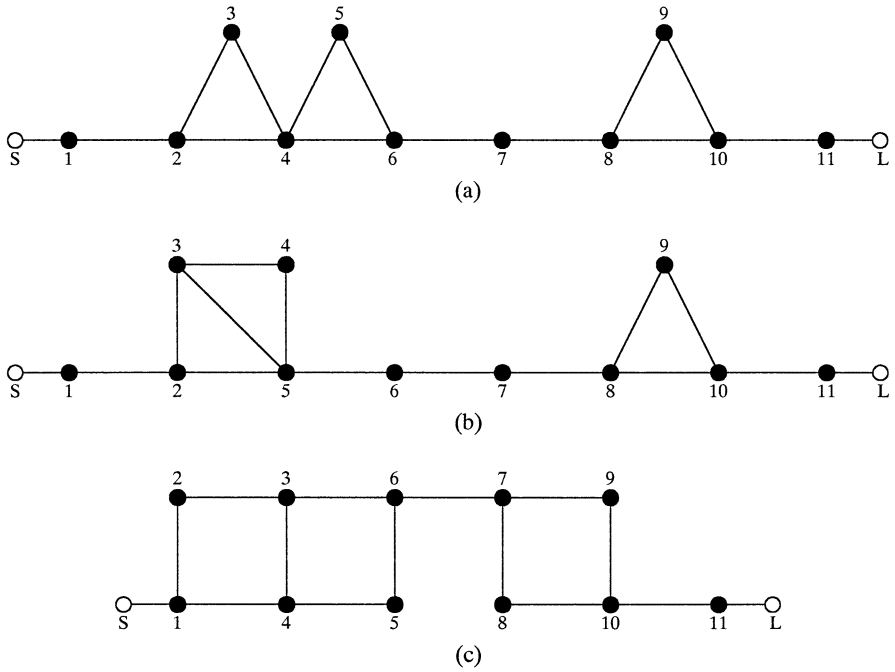

Fig. 11. Stages in the synthesis of an 11–3 network with cascaded box sections. (a) Initial synthesis with trisections. (b) Formation of cascade quad-section. (c) Formation of sixth degree extended box section in cascade with a basic box section.

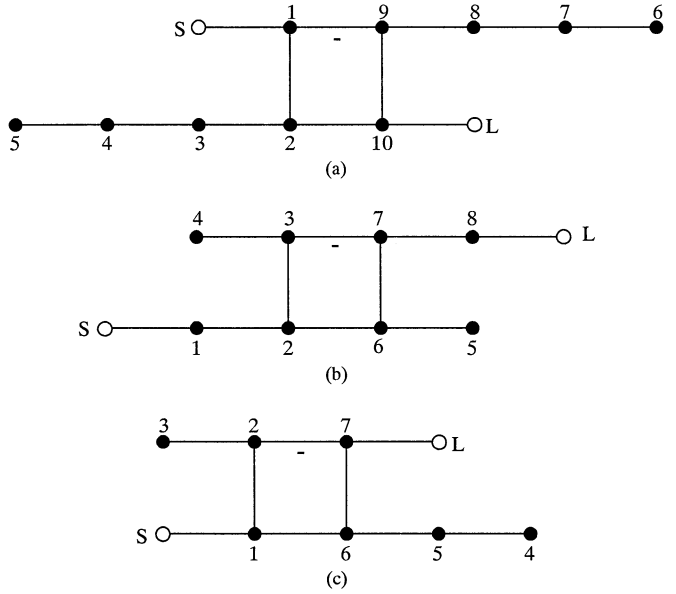

Fig. 12. Cul-de-sac network configurations. (a) 10–3–4 network. (b) 8–3 network. (c) 7–1–2 network.

for symmetric or asymmetric filter responses [7]. This leads to a particularly simple and regular series of rotations, which can be made entirely automatic for any degree of filter. Starting with the folded coupling matrix, elements are annihilated using a series of regular similarity transforms (for odd-degree filters) and cross-pivot transforms (for even-degree filters), beginning with a main-line coupling near the center of the matrix and working outwards along or parallel to the cross-diagonal.

Note that, for cross-pivot annihilations of $M_{ij}(\neq 0)$, where the self-couplings $M_{ii} = M_{jj}$, $\theta_r = \pm\pi/4$ [see (1)]. It is also allowable to have $\theta_r = \pm\pi/4$ for when $M_{ij} = 0$, which will give a slightly different configuration alternative. For odd-degree filters, the angle formula takes the more conventional form

$$\theta_r = \tan^{-1}\left(\frac{M_{i,j-1}}{M_{j-1,j}}\right) \tag{2}$$

where (i, j) is the pivot coordinate.

Table II gives the pivot coordinates and angle formula to be used for the sequence of similarity transforms to be applied to the folded coupling matrix for degrees 4–9 and a general formula for the pivot coordinates for any degree $\geq$4.

The folded-network coupling matrix for the double-terminated version of the example that was used in [2] is shown in Fig. 13(a). This was a seventh degree 23-dB return-loss asymmetric filter, with a complex pair of TZs to give group-delay equalization over approximately 60% of the bandwidth and a single zero on the imaginary axis to give a rejection lobe level of 30 dB on the upper side of the passband.

To transform the folded network coupling matrix to the cul-de-sac configuration, two transformations according to Table II are applied [pivots $[3, 5]$ and $[2, 6]$ with angles calculated from (2)], after which the coupling matrix, as shown in Fig. 13(b), is obtained, corresponding to the coupling and routing diagram of Fig. 12(c). The results of analyzing this coupling matrix are given in Fig. 14(a) (rejection/return loss) and Fig. 14(b) (group delay), where it may be seen that the 30-dB lobe level and equalized in-band group delay have not been affected by the transformation process. Note that when the source and load are directly connected to the corners of the core quartet and the number of finite-position zeros of the prototype is less than $N - 3$, the values of the four couplings in the core quartet have the same absolute value.

TABLE II
PIVOT COORDINATES FOR THE REDUCTION OF THE FOLDED MATRIX TO THE CUL-DE-SAC CONFIGURATION

Degree	Pivot Position $[i, j]$ and Element to be Annihilated Similarity transform number r $r = 1, 2, 3, ..., R$ $R = (N–2)/2$ (N even) $= (N–3)/2$ (N odd)				Transform Angle
N	$r = 1$	2	3	r	θ_r
4	[2,3] M_{23}				eq(1)
5	[2,4] M_{23}				eq(2)
6	[3,4] M_{34}	[2,5] M_{25}			eq(1)
7	[3,5] M_{34}	[2,6] M_{25}			eq(2)
8	[4,5] M_{45}	[3,6] M_{36}	[2,7] M_{27}		eq(1)
9	[4,6] M_{45}	[3,7] M_{36}	[2,8] M_{27}		eq(2)
..	..	..	..	..	..
N (even)	$[i, j]$ $M_{i,j}$ $i = (N + 2)/2 - 1$ $j = N/2 + 1$	..	..	$[i, j]$ $M_{i,j}$ $i = (N + 2)/2 - r$ $j = N/2 + r$	eq(1)
N (odd)	$[i, j]$ $M_{i,j-1}$ $i = (N + 1)/2 - 1$ $j = (N + 1)/2 + 1$	..	..	$[i, j]$ $M_{i,j-1}$ $i = (N + 1)/2 - r$ $j = (N + 1)/2 + r$	eq(2)

	S	1	2	3	4	5	6	7	L
S	0	1.0572	0	0	0	0	0	0	0
1	1.0572	0.0211	0.8884	0	0	0	0	0	0
2	0	0.8884	0.0258	0.6159	0	0	0.0941	0	0
3	0	0	0.6159	0.0193	0.5101	0.1878	0.0700	0	0
4	0	0	0	0.5101	–0.4856	0.4551	0	0	0
5	0	0	0	0.1878	0.4551	–0.0237	0.6119	0	0
6	0	0	0.0941	0.0700	0	0.6119	0.0258	0.8884	0
7	0	0	0	0	0	0	0.8884	0.0211	1.0572
L	0	0	0	0	0	0	0	1.0572	0

(a)

	S	1	2	3	4	5	6	7	L
S	0	1.0572	0	0	0	0	0	0	0
1	1.0572	0.0211	0.6282	0	0	0	0.6282	0	0
2	0	0.6282	–0.0683	0.5798	0	0	0	–0.6282	0
3	0	0	0.5798	–0.1912	0	0	0	0	0
4	0	0	0	0	–0.4856	0.6836	0	0	0
5	0	0	0	0	0.6836	0.1869	0.6499	0	0
6	0	0.6282	0	0	0	0.6499	0.1199	0.6282	0
7	0	0	–0.6282	0	0	0	0.6282	0.0211	1.0572
L	0	0	0	0	0	0	0	1.0572	0

(b)

Fig. 13. Cul-de-sac configuration: seventh degree example. (a) Original folded coupling matrix. (b) After transformation to cul-de-sac configuration.

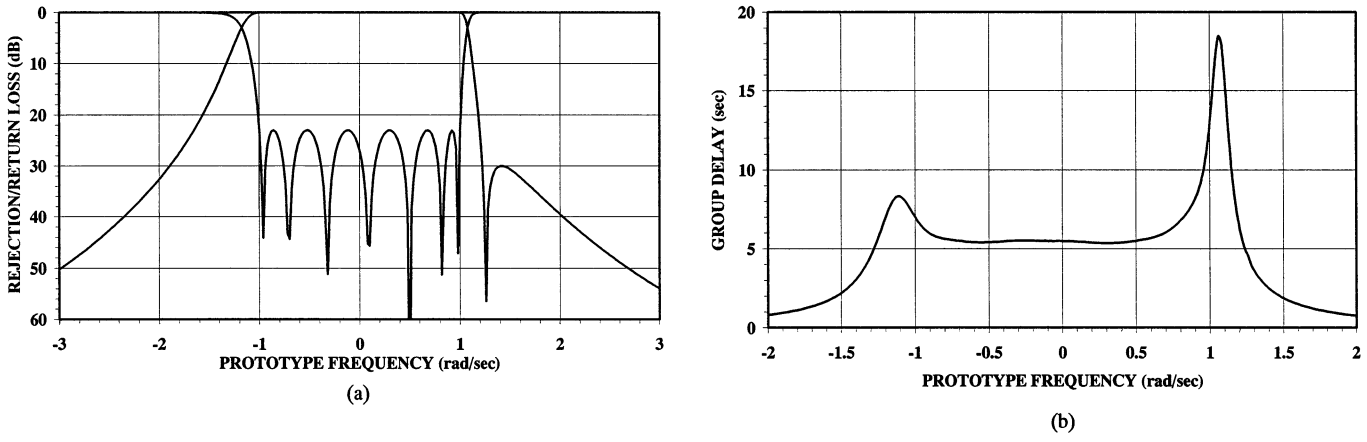

Fig. 14. 7–1–2 asymmetric filter example: simulated performance. (a) Rejection and return loss. (b) Group delay.

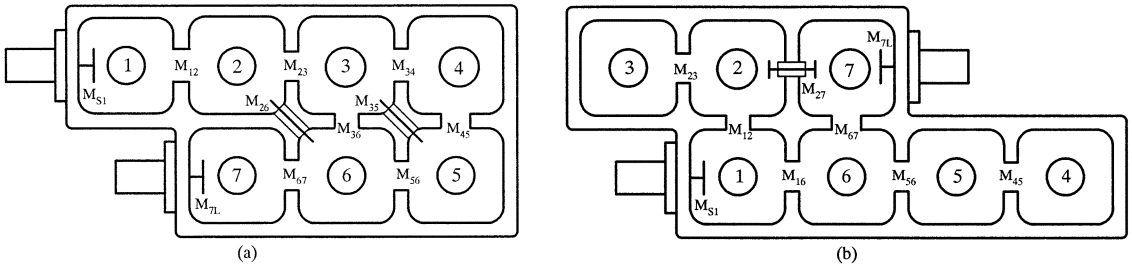

Fig. 15. 7–1–2 asymmetric filter example: coaxial cavity realization configurations. (a) Folded-network configuration. (b) Cul-de-sac configuration.

	S	1	2	3	4	5	6	7	8	L
S	0	1.0428	0	0	0	0	0	0	0	0
1	1.0428	0.0107	0.8623	0	0	0	0	0	0	0
2	0	0.8623	0.0115	0.3744	0	0	–0.4681	0	0	0
3	0	0	0.3744	–0.0439	0.8166	0	0	0.3744	0	0
4	0	0	0	0.8166	0.1976	0	0	0	0	0
5	0	0	0	0	0	–0.9590	0.2093	0	0	0
6	0	0	–0.4681	0	0	0.2093	0.0499	0.4681	0	0
7	0	0	0	0.3744	0	0	0.4681	0.0115	0.8623	0
8	0	0	0	0	0	0	0	0.8623	0.0107	1.0428
L	0	0	0	0	0	0	0	0	1.0428	0

Fig. 16. 8–3 asymmetric filter example. Folded coupling matrix [see Fig. 9(a)] after transformation to cul-de-sac configuration.

The topologies of the filters in coaxial-resonator technology corresponding to the two coupling matrices of Fig. 13 are shown in Fig. 15(a) (folded) and Fig. 15(b) (cul-de-sac), demonstrating the rather simple construction of the cul-de-sac form as compared with the folded form. There are no diagonal cross-couplings and only one negative coupling in the cul-de-sac.

A proof-of-concept S-band model of the same 8–3 prototype as was used for the extended box filter example (Section III) was synthesized in a cul-de-sac configuration, then realized as a coaxial-cavity filter and measured. Starting with the folded coupling matrix for this prototype [see Fig. 9(a)] and applying a series of three cross-pivot transforms at pivots $[4,5]$, $[3,6]$, and $[2,7]$ (Table II) and with angles according to (1), results in the coupling matrix shown in Fig. 16, which corresponds to the configuration of Fig. 12(b). Since the number of finite-position TZs for this prototype was less than the maximum permissible $N-3$, the third transform angle is actually zero and may be omitted for this case.

The simulated and measured rejection and return-loss performances of this filter are shown in Fig. 17, which clearly shows the three TZs. The bandwidth of this filter being quite large (110 MHz) means that the return-loss performance has degraded slightly due to dispersion effects; but these seem to be well predicted by the simulation model.

A sketch of the filter resonator layout is presented in Fig. 18, showing the very uncomplicated coupling arrangement. The omission of the third rotation has left the core quartet $(2,3,6,7)$ not directly connected to the input/output terminations, which should benefit far-out-of-band rejection. This same construction would be able to support eighth degree prototypes with numbers of TZs ranging from nil up to three and with symmetric or asymmetric characteristics.

As was noted above, all the couplings are positive, except for one in the core quartet. This may be moved to any one of the four couplings for the greatest convenience and implemented as a probe, for example, if the filter is to be realized in coaxial-resonator technology, and the other couplings are to be realized as inductive apertures or inductive loops. Also, there are no diagonal couplings even though the original prototype was asymmetric.

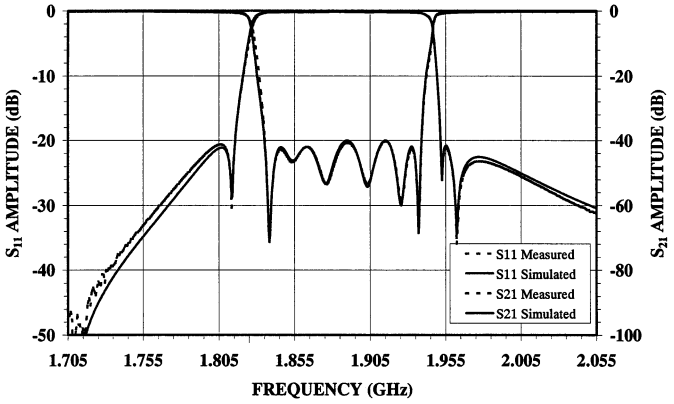

Fig. 17. 8–3 cul-de-sac filter: simulated and measured performance.

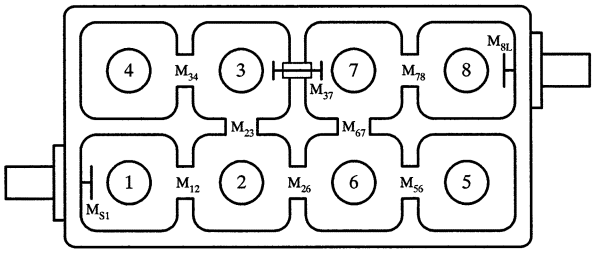

Fig. 18. Cul-de-sac configuration: 8–3 asymmetric filter.

Some of the more important features of the cul-de-sac configuration are summarized as follows.

1) The cul-de-sac topology may be used to realize a completely general class of electrical filtering function, symmetric or asymmetric, even or odd degree, provided that the filtering function is designed to operate between

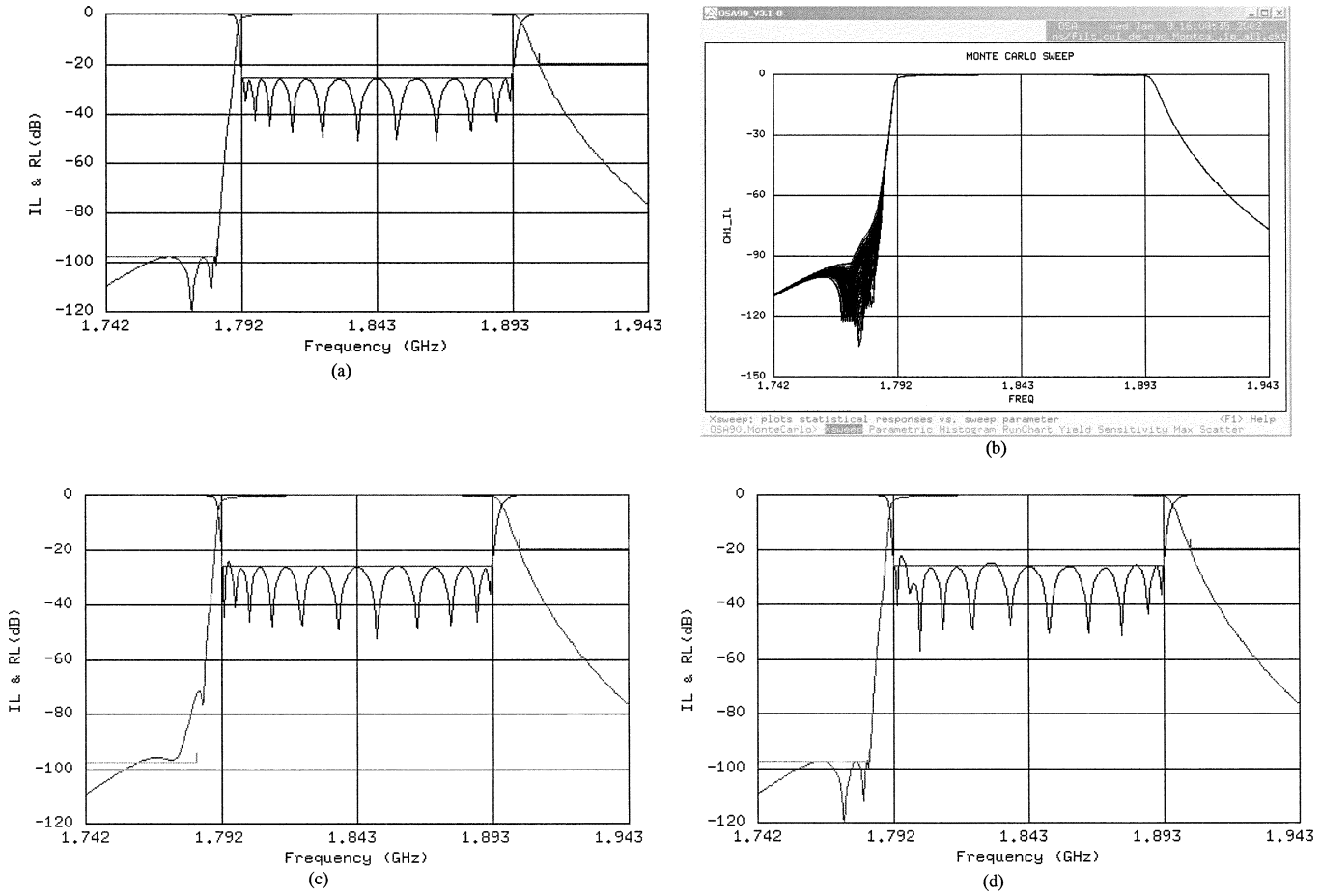

Fig. 19. Sensitivity to variations in coupling value. (a) Nominal 11–3 characteristic. (b) Cul-de-sac: random variations to all couplings. (c) Cul-de-sac: 0.2% increase to self-couplings, 0.2% decrease to all others. (d) Box filter: 0.2% increase to self-couplings, 0.2% decrease to all others.

equal-value source and load terminations ("double-terminated") and that the number of TZs embodied by the filtering function is less than or equal to $N-3$, where N is the degree of the function

2) A given filtering function incorporating TZs may be realized with an absolute minimum number of coupling elements and their associated adjustment mechanisms. e.g., for a tenth degree function with seven TZs, ten internal couplings are required. The equivalent folded structure would need 16 internal couplings, some of which will be diagonal couplings.
3) All the couplings are "straight," i.e., either horizontal or vertical between resonators if these are arranged in a regular grid pattern. This will tend to significantly simplify the design and eliminate the need for diagonal couplings, which are typically difficult to manufacture, assemble, and adjust and tend to be quite sensitive to vibration and temperature variations. The absence of diagonal couplings enables the realization of asymmetric filtering characteristics with dual-mode resonators, e.g., in a dielectric or waveguide and also usage of the high-Q_u TE_{011} cylindrical waveguide resonant mode.
4) The same structure may be used to embody any double-terminated symmetric or asymmetric filtering function of the same degree (provided always that $n_{fz} \leq N-3$). Therefore, the same basic housing incorporating the coupling elements may be used for a variety of filtering characteristics. If the changes in coupling values from the original design are small, e.g., to correct for a dispersion distortion, the changes may be made with tuning and iris adjustment screws without the need to alter the mechanical dimensions of the inter-resonator coupling apertures or to add further cross-couplings.
5) Regardless of the transfer characteristic, all the internal couplings will be of the same sign with the exception of one within the central quartet of resonators. The range over which the values of the internal inter-resonator couplings are spread will be comparatively small, allowing the use of a common design for all the couplings with the same sign.
6) The values of the inter-resonator couplings will be relatively large as compared with the levels of stray and spurious couplings typically found within complex filter structures. This will tend to ease the design and tuning process. Also, the values of all inter-resonator couplings are externally adjustable with screws, reducing the need for tight tolerances during manufacture and enabling optimal performance to be obtained during production.
7) The Q_u-factor of a microwave resonant cavity tends to decrease as the number of coupling elements interconnecting to it increases, thus, increasing the insertion loss of the filter of which it forms a part. Since there are

a minimal number of inter-resonator couplings in the cul-de-sac filter and only one of those is a negative coupling (which tend to be realized as a probe in coaxial and dielectric filters and can be relatively lossy, particularly if it is a diagonal coupling), its insertion loss will be less than the equivalent filter with more coupling elements.

8) By short-circuiting certain cavities, the filter may be split into smaller sections, which will tend to ease the development and production tuning processes.
9) The cul-de-sac filter may be manufactured as a simple two-dimensional two-part housing + lid assembly with all the tuning screws on top, making it very suitable for mass production and tuning methods. The form is also amenable to volume manufacturing processes such as die casting. A certain amount of flexibility is available in the layout of its cavities, enabling compact integration with other subsystems and components in the same system.

A. Sensitivity Considerations

Having the minimum number of internal couplings, it is to be expected that the cul-de-sac filter will be more sensitive to variations in its coupling element values and tuning state than the equivalent filter realized in the folded configuration or with trisections, etc. To assess the nature of this sensitivity and to make a comparison with alternative configurations realizing the same filtering function, a brief qualitative simulation study was made.

There will be two main classes of variation in the coupling and resonator tuning states, i.e., random, which will be due to component and manufacturing/assembly tolerances, and unidirectional or bidirectional, which will be caused by temperature fluctuations during operation.

The first category was assessed using a Monte Carlo sensitivity analysis package on an eleventh degree characteristic with three TZs on the lower side giving 97-dB rejection lobe levels, realized in folded box section [see Fig. 11(c)], trisection, and cul-de-sac configurations. Here, the box and trisection were relatively little affected by 1% standard deviation variations in coupling values alone, but the rejection performances of the folded and cul-de-sac were both quite seriously affected [see Fig. 19(b)]. Although the variations in the values in the coupling elements will be adjustable during production with tuning screws, counteracting the effect of manufacturing and assembly tolerances and restoring the rejection performance, there will be an impact on volume production where more careful and accurate tuning will be required.

The second category of variation was investigated by applying a 0.2% increase to self-couplings and a 0.2% decrease to the other coupling values. Here, the cul-de-sac fared worst overall with the rejection performance suffering significantly [see Fig. 19(c)]. By comparison, the box filter is relatively lightly affected [see Fig. 19(d)]. This indicates that greater thermal stability of the coupling values and resonant frequencies of cul-de-sac filters will be required or that the mechanical design gives shifts in the same direction under the influence of temperature changes.

V. Conclusion

In this paper, the exact synthesis methods for two novel configurations for microwave filters have been introduced, i.e., the box (and its extended form) and the cul-de-sac forms. The new forms feature some important constructional simplifications that should ease the volume production process for high-performance microwave filters for the wireless industry and make practical the realization of a wide range of advanced asymmetric filtering characteristics in dual- or triple-mode technology without an accompanying increase in constructional complexity.

Acknowledgment

The authors are grateful to Dr. M. Yu, COM DEV Canada, Cambridge, ON, Canada, for performing the comparative sensitivity study for filters in the various configurations, the results of which are summarized in this paper.

References

[1] R. J. Cameron, "General prototype network-synthesis methods for microwave filters," *ESA J.*, vol. 6, pp. 193–206, 1982.
[2] ——, "General coupling matrix synthesis methods for Chebyshev filtering functions," *IEEE Trans. Microwave Theory Tech.*, vol. 47, pp. 433–442, Apr. 1999.
[3] A. E. Atia and A. E. Williams, "Narrow-bandpass waveguide filters," *IEEE Trans. Microwave Theory Tech.*, vol. MTT-20, pp. 258–265, Apr. 1972.
[4] A. E. Atia, A. E. Williams, and R. W. Newcomb, "Narrow-band multiple-coupled cavity synthesis," *IEEE Trans. Circuits Syst.*, vol. CAS-21, pp. 649–655, Sept. 1974.
[5] R. J. Cameron and J. D. Rhodes, "Asymmetric realizations for dual-mode bandpass filters," *IEEE Trans. Microwave Theory Tech.*, vol. MTT-29, pp. 51–58, Jan. 1981.
[6] A. E. Williams, J. I. Upshur, and M. M. Rahman, "Asymmetric response bandpass filter having resonators with minimum couplings," U.S. Patent 6 337 610, Jan. 8, 2002.
[7] H. C. Bell, "Canonical asymmetric coupled-resonator filters," *IEEE Trans. Microwave Theory Tech.*, vol. MTT-30, pp. 1335–1340, Sept. 1982.

Richard J. Cameron (M'83–SM'94–F'02) was born in Glasgow, U.K., in 1947. He received the B.Sc. degree in telecommunications and electronic engineering from Loughborough University, Loughborough, U.K., in 1969.

In 1969, he joined Marconi Space and Defence Systems, Stanmore, U.K. His activities there included small earth-station design, telecommunication satellite system analysis, and computer-aided RF circuit and component design. In 1975, he joined the European Space Agency's technical establishment (ESTEC, The Netherlands), where he was involved in the research and development of advanced microwave active and passive components and circuits, with applications in telecommunications, scientific, and earth observation spacecraft. Since joining COM DEV International Ltd., Aylesbury, U.K., in 1984, he has been involved in the software and methods for the design of a wide range of high-performance components and subsystems for both space and terrestrial application.

Mr. Cameron is a Fellow of the Institution of Electrical Engineers (IEE), U.K.

A. R. Harish (M'00) received the Ph.D. degree in electrical engineering from the Indian Institute of Technology, Kanpur, India, in 1997.

From 1997 to 2000, he was a Senior Engineer, and from 2000 to 2002, he was the Chief RF Passive Engineer with COM DEV Wireless, Dunstable, U.K. From March 2002 to July 2002, he was the Chief RF Passive Engineer with Mitec Telecom Ltd., Dunstable, U.K. Since July 2002, he has been a Visiting Assistant Professor with the Department of Electrical Engineering, Indian Institute of Technology. His current research concerns the application of efficient numerical and optimization techniques for computer-aided design (CAD) of microwave circuits and antennas, analysis, and synthesis of microwave filters.

Christopher J. Radcliffe (M'87) received the B.Sc. degree in physics and M.Sc. degree in radio astronomy from Manchester University, Manchester, U.K., in 1967 and 1969, respectively.

In 1970, he joined Marconi Space and Defence Systems, where he was involved with communication satellite system design. He then spent several years involved with the development of linear phase filters for the European Communications Satellite (ECS) series, both as a Designer and Project Manager. He was then involved in the design and production of advanced coaxial and waveguide filters for military earth stations. The specifications for these devices included stringent requirements for high-power handling, linear phase, and very low passive intermodulation levels. He was the Group Leader with Marconi Space and Defence Systems for a number of years, during which time he was responsible for all the RF and microwave filter work, including research with the European Space Agency (ESA). In 1984, he left Marconi Space and Defence Systems to co-found the Phase Devices Company as Technical Director, where he was involved in the design and development of a large range of coaxial and waveguide filters, diplexers, and other passive devices for the cellular communication market. These included linear phase filters, asymmetric filters, and diplexers with multiple stop poles and dual-mode tunable combiners for cellular telephoning base stations. He is currently a consultant with a specialization in microwave filter design for space and terrestrial applications.